Article

The Role of the Bridge in Single-Ion Magnet Behaviour: Reinvestigation of Cobalt(II) Succinate and Fumarate Coordination Polymers with Nicotinamide

Marek Brezovan [1], Jana Juráková [2] , Ján Moncol [1], Ľubor Dlháň [1], Maria Korabik [3], Ivan Šalitroš [1,2,4], Ján Pavlik [1,*] and Peter Segľa [1]

[1] Faculty of Chemical and Food Technology, Slovak University of Technology, Radlinského 9, 81237 Bratislava, Slovakia
[2] Central European Institute of Technology, Brno University of Technology, Purkyňova 123, 61200 Brno, Czech Republic
[3] Faculty of Chemistry, University of Wrocław, F. Joliot-Curie 14, 50-383 Wrocław, Poland
[4] Faculty of Science, Palacký University, 17. Listopadu 12, 77146 Olomouc, Czech Republic
[*] Correspondence: jan.pavlik@stuba.sk

Abstract: Two previously synthesized cobalt(II) coordination polymers; $\{[Co(\mu_2\text{-suc})(nia)_2(H_2O)_2]\cdot 2H_2O\}n$ (suc = succinate(2−), nia = nicotinamide) and $[Co(\mu_2\text{-fum})(nia)_2(H_2O)_2]n$ (fum = fumarate(2−)) were prepared and thoroughly characterized. Both complexes form 1D coordination chains by bonding of $Co(nia)_2(H_2O)_2$ units through succinate or fumarate ligands while these chains are further linked through hydrogen bonds to 3D supramolecular networks. The intermolecular interactions of both complexes are quantified using Hirshfeld surface analysis and their infrared spectra, electronic spectra and static magnetic properties are confronted with DFT and state-of-the-art ab-initio calculations. Dynamic magnetic measurements show that both complexes exhibit single-ion magnet behaviour induced by a magnetic field. Since they possess very similar chemical structure, differing only in the rigidity of the bridge between the magnetic centres, this chemical feature is put into context with changes in their magnetic relaxation.

Keywords: single-ion magnet; cobalt(II) coordination polymer; ab-initio calculations

1. Introduction

Coordination polymers have been studied for a long time in terms of architecture, topology, and their potential applications in catalysis [1–3], gas adsorption [4–6], chemical adsorption [7], luminescence [8,9], and design of molecular magnetic materials [10–12]. The proper choice of relevant ligands and metal centre is the key to form fascinating and useful coordination polymers [13–23].

An extremely appealing class of molecular magnetic materials is formed by *single-molecule magnets* (SMMs) [24]. Very simply speaking, in these materials, the magnetic dipole moments tend to keep their orientation with respect to the molecular or polymeric frame. In reality, however, any imposed orientation disappears after some time, mostly due to their interference with thermal bath of molecular surroundings. In current SMMs it happens typically within milliseconds, albeit the limit of second has already been breached [25]. This measurable process is called *slow relaxation of magnetization* and its time constant is used as a characteristic of SMM systems. In special cases of 1D polymers, the term *single-chain magnets* (SCM) is used [26]. In both SMMs and SCMs, the slow relaxation of magnetization exists as a collective property of the magnetic centres. If, on the other hand, magnetically isolated centres are capable of slow relaxation of magnetization, a *single-ion magnet* (SIM) is encountered [27]. Counterintuitively, the chemical and magnetic structure of a system need not coincide, one can find, e.g., a chain of SIMs [28]. Although the best performing SIMs are based on the

lanthanide and actinide central atoms [29], among few suitable 3*d*-elements, cobalt (II) occupies a prominent position forming SIMs with two-, three- four-, five-, six-, seven- and eight-coordinate Co(II) centres and various geometries of coordination environment [30]. The vast majority of them, however, are six-coordinate, which is thanks to the high unquenched angular momentum they bear [31]. The role of the angular momentum and symmetry of coordination environment plays important role for the mechanism of magnetic relaxation and there is a lot of attention being paid to the fine tuning of the relaxation process by design of the coordination environment. For example, the effect of linearity of coordinated pseudohalides was systematically addressed by Herchel et al. [32] or Wang et al. [33], and distortion of octahedral coordination environment was studied by groups of Pardo [34], Gao [35], Song [36,37], Herchel [38,39], or Colacio [40], concluding sometimes that the closest environment of Co(II) ion is decisive for SIM behaviour [41]. Nevertheless, there occur some clues that the focus on the central atom itself cannot uncover the full story behind slow relaxation of magnetization in SIMs. As discussed e.g., by Ren et al. [42] or Boča et al. [43] and very explicitly stated by Dunbar et al. [44]: " . . . *the deciding factor for SMM behavior is not the degree of distortion which, a priori, would be expected to be the case, but rather the interactions between neighboring molecules in the solid state*". Nonetheless, the stiffness of molecular and supramolecular structures is somehow overlooked in this context and the research in this sake is almost exclusively theoretical [29]. In one of very scarce works, Marinho et al. synthesized by carefully controlled conditions four variants of Co(II) coordination polymer which differed in their folding. The conformation of bridges manifested itself in the relaxation of the chain-arranged SIMs [45]. However, to the best of our knowledge no study yet addressed the question of the effect of rigidity of bridges connecting SIM centres.

Keeping this in mind, herein we attempted to compare the effect of bridge saturation upon the SIM behaviour in two analogous Co(II) coordination polymers. The succinate polymer $\{[Co(\mu_2\text{-suc})(nia)_2(H_2O)_2]\cdot 2H_2O\}_n$ (suc = succinate(2−), nia = nicotinamide, complex **I**) was synthesized in 2009 by Demir et al. and characterized by single-crystal X-ray crystallography, IR spectroscopy, photoluminescence and TG-DTA [46]. The fumarate polymer $[Co(\mu_2\text{-fum})(nia)_2(H_2O)_2]_n$ (fum = fumarate(2−), complex **II**) was prepared in 2018 by Kansız et al. and characterized by FT-IR, X-ray crystallography and DFT calculations [47].

We demonstrated an alternative synthetic route for complex **I** employing *N*-(hydroxym ethyl)nicotinamde (hmnia) instead of nicotinamide. Crystal structures of both complexes were refined using aspheric atomic scattering factors by Hirshfeld Atomic Refinement and analysed using Hirshfeld surface analysis. Infrared and electronic spectra were interpreted and confronted with the prediction from DFT. The magnetic properties of complexes were measured and thoroughly interpreted with assistance of state-of-the-art quantum chemistry method CASSCF-NEVPT2-SOI. Finally, magnetic relaxation was discussed for these systems in context of mutual variances in their chemical structure.

2. Results

2.1. Syntheses and Characterization

Direct preparation of polymeric cobalt(II) carboxylates from nicotinamide—nia is represented in Scheme 1. Complex $\{[Co(\mu_2\text{-suc})(nia)_2(H_2O)_2]\cdot 2H_2O\}_n$ (**I**) was also prepared from *N*-(hydroxymethyl)nicotinamide—hmnia (Scheme 2). Such a tendency of Co(II) salts to degradation of hmnia was not yet described in literature despite the fact that only very few Ni(II), Co(II) and Cu(II) complexes with hmnia are known [48–50]. A similar reaction occurs in the Chłopicki's preparation of the pyridinium salts of nicotinamide [51]. In Chłopicki's procedure the nitrogen atom of the amide group of nicotinamide is protected with methanal and after subsequent alkylation at the pyridine nitrogen atom, the methanal is released in water media at 37 °C. Cobalt (II) dichloride serves as Lewis acid, coordinating the pyridine nitrogen atom (instead of quarternization like it was in the patent) thus enabling easier methanal release (Scheme 2). In contrast with Chłopicki's procedure, however, in our case the reaction mixture was refluxed for two hours.
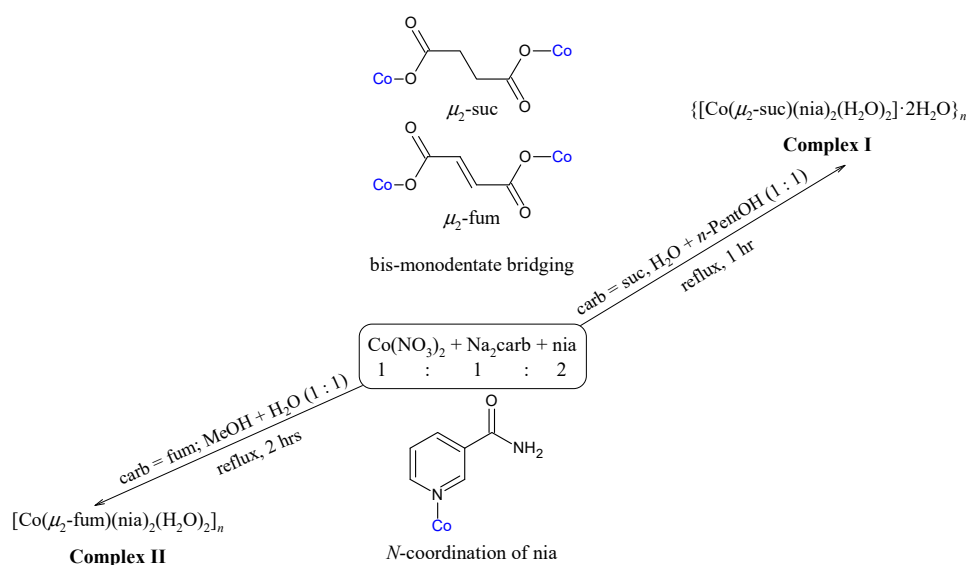
Scheme 1. Synthesis of polymeric cobalt(II)dicarboxylate complexes (**I** and **II**) from nicotinamide.
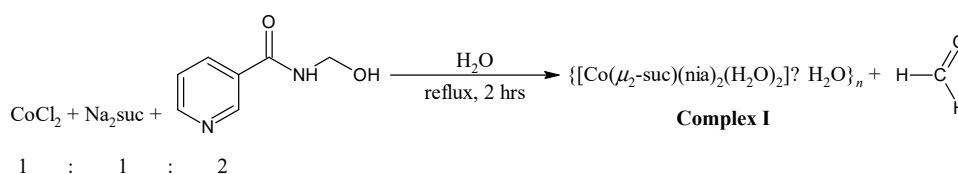
Scheme 2. Synthesis of polymeric cobalt(II)succinate complex (**I**) from N-(hydroxymethyl) nicotinamide.

The preparation of complexes **I** and **II** was carried out by short refluxing from a water + n-pentanol (complex **I**, prepared from nia, Scheme 1), water + methanol (complex **I**, prepared from hmnia, Scheme 2) and water solution (complex **II**). The molar ratio of the reactants was 1:1:2 for cobalt(II) salts, sodium salts of dicarboxylic acids and nicotinamide or N-(hydroxymethyl)nicotinamide, respectively. To synthesize the discussed complexes, various molar ratios of cobalt(II) chloride hexahydrate or cobalt(II) nitrate hexahydrate to sodium carboxylate (succinate or fumarate)—Na$_2$carb (where carb is suc or fum anion) and corresponding nicotinamide or N-(hydroxymethyl)nicotinamide were tested, specifically 1:1:1; 1:2:1; 1:1:2 and 1:2:2. Well-defined crystalline products were obtained only for the case of 1:1:2 (Schemes 1 and 2). The syntheses of complexes **I** and **II** was very well reproducible in terms of the product quality and yield. Prepared complexes are non-hygroscopic and stable in air and soluble in hot water.

2.2. Description of the Structures

The crystal structure of both compounds **I** and **II** was previously determined using standard single-crystal X-ray diffraction at room temperature, and their models were refined using the standard IAM [46,47]. In this study, the structural parameters of both compounds are significantly more accurate as they were obtained by refining the structure model (all H atoms being refined isotropically and independently) using aspheric atomic scattering factors and the HAR method. Selected bond distances are given in Table S2 (see Supplementary Materials).

The cobalt atoms of both complexes lie in the centre of symmetry and are octahedrally coordinated by two oxygen atoms (O1) of the carboxyl groups of the succinate (**I**) [Co1–O1 = 2.0931(9) Å] or fumarate (**II**) [Co1–O1 = 2.0683(8) Å] anionic ligands, two nitrogen atoms (N1) of the pyridine rings of the nicotinamide ligands [Co1–N1 = 2.1672(12) Å for **I** and 2.1689(10) Å for **II**], and a pair of oxygen atoms (O1W) of the coordinated water

molecules [Co1–O1W = 2.1090(10) Å for **I** and 2.0924(9) Å for **II**] in trans positions (Figure 1). Both substances form 1D coordination chains formed by bonding of Co(nia)$_2$(H$_2$O)$_2$ units bridged through succinate (**I**) or fumarate (**II**) ligands. The closest Co$\cdots$Co distances are 9.465 Å in **I** and 9.740 in **II**.
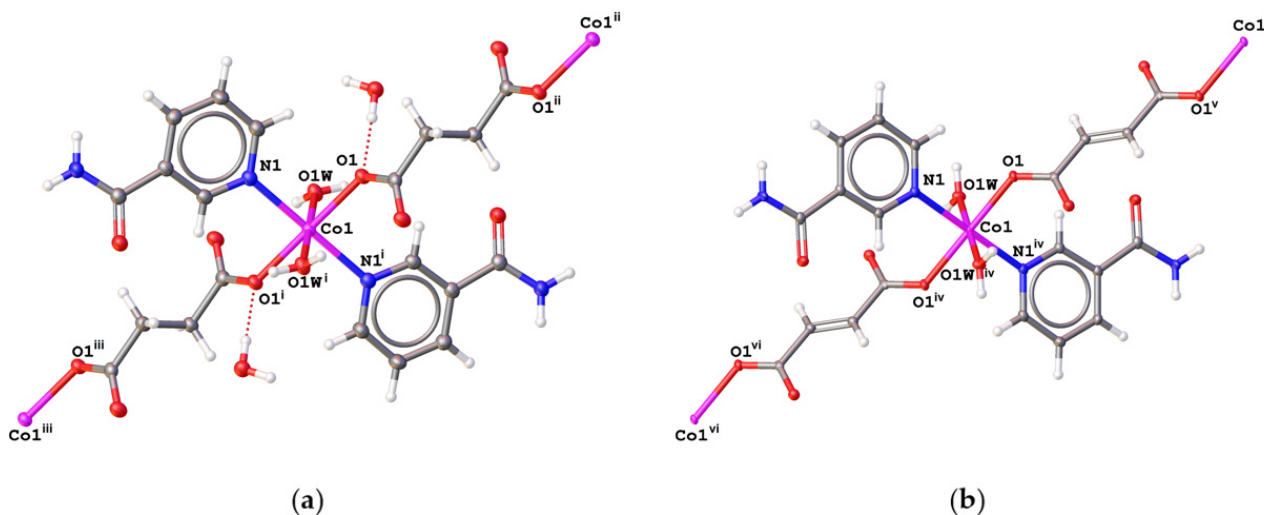

Figure 1. Comparison of perspective view of the molecular structure of the complexes: (**a**) **I** and (**b**) **II**. Thermal ellipsoids are drawn at the 50% probability level. Symmetry codes: (i) $1 - x$, $1 - y$, $2 - z$; (ii) $-x$, $2 - y$, $2 - z$; (iii) $1 + x$, $-1 + y$, $+z$; (iv) $1 - x$, $1 - y$, $-z$; (v) $-x$, $-y$, $-z$; (vi) $1 + x$, $1 + y$, $+z$.

Several ideal six-coordinate geometries were compared with **I** and **II** through SHAPE structural analysis, proposed by S. Alvarez et al. [52–55] (Table S3, see Supplementary Materials). The obtained symmetry measure parameters undoubtedly prove the octahedral shape of coordination polyhedra of reported compounds (S(O_h) ≈ 0.2 for **I** and 0.3 for **II**) and the next lowest values for the trigonal prism shape (S(D_{3h}) ≈ 16.1 for both **I** and **II**) suggest that the Bailar twist does not occur in the reported complexes. Furthermore, the distortion parameter Σ [56,57], calculated from the twelve *cis* angles of the hexacoordinated polyhedron (Table S3, see Supplementary Materials) acquiring zero values when ideal octahedral symmetry is present, can express the degree of angular distortion of coordination polyhedra of reported compounds. Both reported complexes indicate only moderate angular distortion, although more pronounced in the complex **II** ($\Sigma = 43°$), since its value of distortion parameter is notably higher comparing the one observed in **I** ($\Sigma = 30°$).

The 1D coordination chains of both complexes are linked through hydrogen bonds to 3D supramolecular hydrogen-bonding networks. Parameters of hydrogen bonds are given in Table S4 (see Supplementary Materials). Figure S1 (see Supplementary Materials) shows the O–H$\cdots$O hydrogen bonds between the two 1D coordination chains of compound **I** (top) and compound **II** (bottom). Two coordination chains of **I** are joined via O–H$\cdots$O hydrogen bonds between coordinated water molecules (O1W) and oxygen atoms (O2) of the carboxyl groups of succinate anions of adjacent coordination chains [O1W–H1WB$\cdots$O2, with O$\cdots$O distance of 2.857(1) Å (Table S4, see Supplementary Materials)]. The oxygen atoms (O1W) of coordinated water molecules are linked by O–H$\cdots$;O hydrogen bonds to the oxygen atoms of uncoordinated water molecules (O2W) [O1W–H1WA$\cdots$O2W, with O$\cdots$O distance of 2.758(1) Å]. Uncoordinated water molecules (O2W) are further involved as donor atoms in other O–H$\cdots$O hydrogen bonds where the oxygen atoms (O1) of carboxyl groups [O2W–H2WA$\cdots$O1, with O$\cdots$O distance of 2.794(1) Å], and oxygen atoms (O3) of carboxamide groups of nicotinamide ligands [O2W–H2WB$\cdots$O3, with O$\cdots$O distance of 2.834(1) Å] serve as acceptor atoms of H-bonds. On the other hand, the O–H$\cdots$O hydrogen bonds in crystal structure of **II** are observed only between the oxygen atoms (O1W) of the coordinated water molecules and the oxygen atoms (O2) of the carboxyl groups of fumarate anions [O1W–H1WB$\cdots$O2, with O$\cdots$O distance of 2.758(1) Å], and between the

oxygen atoms (O1W) of the coordinated water molecules and the oxygen atoms (O3) of carboxamide groups of nicotinamide ligands [O1W–H1WA···O3, with O···O distance of 2.822(1) Å].

The N–H···O and C–H···O hydrogen bonds of both complexes are shown in the Figures S2 and S3 (see Supplementary Materials). Crystal structures of both complexes show formation of supramolecular rings $R_2^2(8)$ [58] by linking two carboxamide groups via a pair of N–H···O hydrogen bonds [N2–H2A···O3, with N···O distance of 2.943(1) Å for **I** and 2.972(1) Å for **II**, (Table S4 and Figure S2, see Supplementary Materials)]. The crystal structure of **II** also shows π-π stacking interactions of the pyridine rings [N1/C2–C5] of nicotinamide ligands (distances between two planes of 3.52 Å, centroid-centroid distance of 3.95 Å, shift distance of 1.77 Å [59]). In Figure S3 (see Supplementary Materials) the supramolecular rings $R_2^1(7)$ [58] observed in the crystal structure of both complexes is displayed. These supramolecular rings form nicotinamide molecules and oxygen atoms (O2) of carboxylate groups of succinate (**I**) or fumarate (**II**) ligands through N–H···O hydrogen bonds between nitrogen atom (N2) of carboxamide group of nicotinamide ligand and carboxylate oxygen atom (O2) [N2–H2B···O2, with N···O distance of 3.046(1) Å for **I** and 2.901(1) Å for **II**, (Table S4 and Figure S3, see Supplementary Materials)], and C3–H3···O2 hydrogen bonds between carbon atom (C3) of pyridine ring of nicotinamide ligand and carboxylate oxygen atom (O2) [C3–H3···O3, with C···O distance of 3.357(1) Å for **I** and 3.232(1) Å for **II**].

2.2.1. Hirshfeld Surface Analysis

The intermolecular interactions of both complexes have been quantified using Hirshfeld surface analysis. Figures S4 and S5 (see Supplementary Materials) show transparent 3D Hirshfeld surface mapped over d_{norm} shape index for complex **I** and complex **II**, respectively. Deep red spots on these surfaces indicate close-contact interactions majority of which is due to intermolecular hydrogen bonds. In the case of **II** π-π stacking interactions between pyridine rings of nicotinamide ligands are also visible (Figure S5, see Supplementary Materials). As shown in the 2D fingerprint plots (Figures S6 and S7, see Supplementary Materials), H···H interactions cover 37.3–40.6% range of the total Hirshfeld surface, H···O/O···H interactions span between 31.1–35.3%, H···C/C···H interactions cover between 9.1 and 11.1% and C···C interactions between 9.0 and 10.6%.

2.2.2. X-ray Powder Diffraction

The Le Bail analysis of both samples shows that they are of good crystalline quality without any significant amount of foreign impurity (Figures S8 and S9, see Supplementary Materials). A small residual intensity in difference plot can be assigned to the effect of real structure of powder sample. For example, artifacts of "first derivative" shape on difference plot originate from peak asymmetry of strong diffraction lines at low angle region. It can be concluded that both powder samples of **I** and **II** possess the same crystal structure as the structure of the corresponding single crystals.

2.3. Spectral Characterization

Infrared spectra of complexes **I** and **II** comprise bands confirming the presence of all characteristic functional groups. Some characteristic bands in the IR mid region of the nicotinamide (nia), the sodium salts (Na$_2$suc·6H$_2$O and Na$_2$fum) and cobalt(II) complex **I** (prepared from nia and hmnia) and complex **II** are given in Table S5 (see Supplementary Materials).

IR spectra of model molecules **1** and **2** (Figures S10–S12, see Supplementary Materials) were calculated at the B3LYP/def2-TZVP level of theory after successful geometry optimization. Comparison of experimental and theoretical IR spectra is displayed in Figures S10–S12 and assigned bands of both complexes are collected in Table S5 (see Supplementary Materials).

In the IR spectra of **I**, **II** and Na$_2$suc·6H$_2$O the broad bands at ca. 3500 cm^{-1} were assigned to ν(O–H) groups from coordinated and uncoordinated water molecules [60].

In theoretical spectra of **1** and **2** the O–H stretching modes were recorded at 3653 and 3628 cm^{-1} (Table S5, see Supplementary Materials).

In the experimental IR spectra of **I**, **II** and nia, the bands assigned to the symmetric and antisymmetric stretching vibrations of NH$_2$ groups from nicotinamide are observed in region about 3400–3140 cm^{-1} (Table S5, see Supplementary Materials). In calculated spectra only symmetric ν_s(NH$_2$) (and none antisymmetric) stretching vibration modes were obtained at 3293 cm^{-1} for both model molecules.

The C–H aromatic stretching modes are observed in experimental spectra at the same wavenumber 3062 cm^{-1}, while calculation gives 3012 cm^{-1} (complex **I**) and 3018 cm^{-1} (complex **II**). Aliphatic stretching vibrations are observed only for complex **I**, the antisymmetric ν_{as}(CH$_2$) at 2988 cm^{-1} and symmetric ν_s(CH$_2$) at 2955 cm^{-1} while the calculation predicts 2957 cm^{-1} and 2939 cm^{-1}, respectively (Table S6, see Supplementary Materials).

Most characteristic bands for dicarboxylate complexes are due to symmetric ν_s(COO$^-$) and antisymmetric ν_{as}(COO$^-$) stretching vibrations of carboxylate groups [61]. While the former are observed at ca. 1370 cm^{-1}, the latter occur at ca. 1560 cm^{-1} (Table S5, see Supplementary Materials). The difference (Δ) between the wavenumber of antisymmetric and symmetric vibration of carboxylate group gives information on the carboxylate bonding mode of complexes. When confronted with disodium succinate (141 cm^{-1}) and disodium fumarate (188 cm^{-1}) which possess ionic carboxylic groups, complexes **I** and **II** show higher values of Δ (180 cm^{-1} and 201 cm^{-1}, respectively) which are typical for monodentate *O*-coordination of carboxylate groups [61]. Bis(monodentate) bridging coordination mode of both carboxylate group in all complexes agrees with the structure of complexes as was determined by X-ray analysis.

In the recorded experimental IR spectra for the nia as well as for the complexes under study very strong or strong bands at about 1670, 1620 and 1390 cm^{-1} were assigned to Amide I (mainly ν(C=O)), Amide II (mainly δ(NH$_2$)) and Amide III (mainly ν(C–N) stretching) (S4). The vibration mode of Amide II and Amide III was calculated at about 1610 and 1370 cm^{-1}, respectively (Table S6, see Supplementary Materials). Relatively close positions of the bands assigned to Amide I, Amide II and Amide III for complexes under study to positions of bands in corresponding free molecules of nicotinamide are typical for non-coordinated amide groups [60].

In the UV-Vis absorption spectra, bands at about 220 and 265 nm can be observed, which are assigned to ligand (suc, fum and nia) internal transitions (Figures S13–S15, see Supplementary Materials). The shoulder at 350 nm is assigned to ligand-to-metal charge transfer transition [62] (LMCT, OαCo, NαCo). A band in the visible region between 470 and 480 nm with shoulder between 490 and 506 nm can be assigned to the $^4T_{1g}$(F) $\rightarrow$ $^4T_{1g}$(P) transition. Obtained electronic spectra are consistent with a strict-octahedral or a tetragonally-distorted-octahedral structure of coordination environment [63].

The electronic spectra of model molecules **1** and **2** were calculated at the same level of theory like the IR spectra. Only one dominant absorption was found for both cases, centred at 354 nm for **1** and 357 nm for **2** (Figure S16, Table S7, see Supplementary Materials). Inspection of the natural transition orbitals (NTOs) [64] associated with this electronic transition suggests that it corresponds to metal-to-ligand charge transfer in both cases (Figure S17, see Supplementary Materials) In both cases, a corresponding peak can be found in the experimental spectra, overlaid by strong intraligand absorption peak.

2.4. Static Magnetic Properties

Magnetic behaviour of complexes **I** and **II** is displayed in Figure 2. In general, the decrease of magnetic moment with decreasing temperature is mostly due to local magnetic anisotropy and/or magnetic coupling interaction. Usually, the simple isotropic form of the interaction is applicable for octahedral Co(II) complexes [65]. A DFT assessment on model systems **11** and **22** (Figure S18, Table S8, see Supplementary Materials) indicated however its negligible contribution and studied systems cannot be considered single-chain magnets. The local magnetism of Co(II) complexes with octahedral coordination environment is

governed by both, spin magnetic momentum and angular magnetic momentum of the ground state [66]. Nevertheless, in some cases the angular momentum can be omitted, and it can be effectively described by simple spin Hamiltonian. As a rule of thumb this approximation can be applied if two lowest Kramers' doublets of the ground term $^4T_{1g}$ are separated from excited doublets by more than 1000 cm^{-1} [67].

(a)   (b)
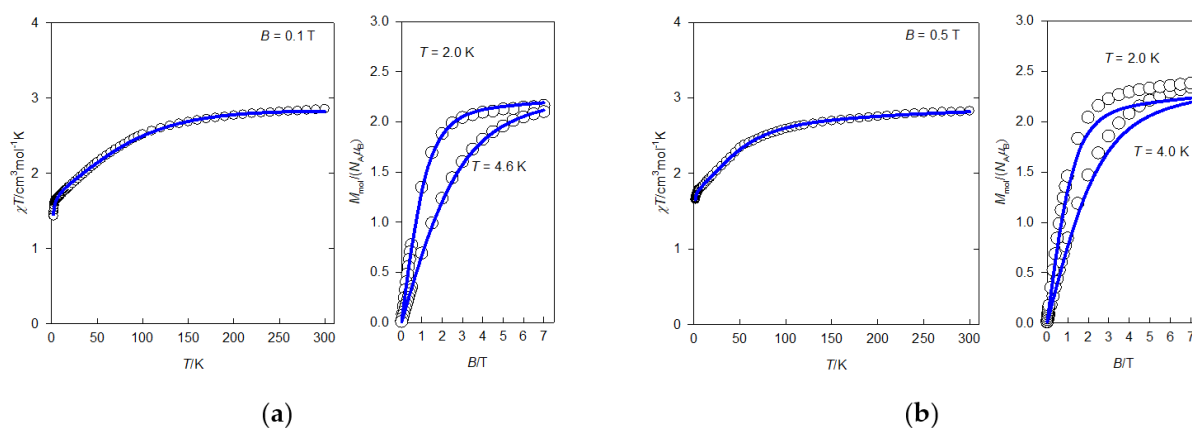
Figure 2. Product of magnetic susceptibility and temperature as a function of temperature (left) and magnetization as a function of magnetic field (right) per one magnetic centre for: (**a**) **I** and (**b**) **II**. Circles: experiment, solid line: optimum parameter fit.

To obtain this kind of insight, the magnetic energetic levels of mononuclear model systems **1** and **2** (Figure 3) were inspected using the method SA-CAS[7,5]SCF-NEVPT2-SOI. The resulting energy values of relevant Kramers' doublets are presented in Table S9 (see Supplementary Materials) revealing that the spin Hamiltonian is not justified in these systems (separation of Γ_c and Γ_b by 420.1 cm^{-1} and 272.9 cm^{-1} for **1** and **2**, respectively).

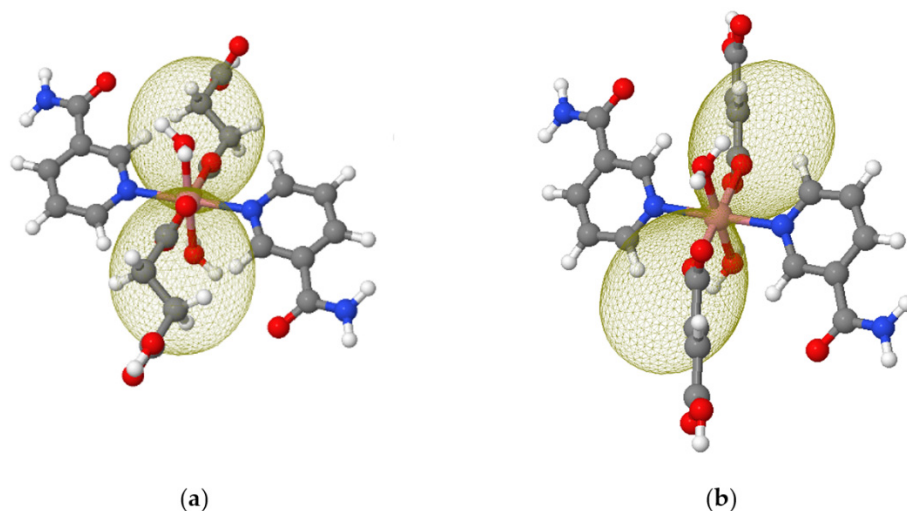(a)   (b)

Figure 3. A cut-off from respective polymeric systems **I** and **II** forming a neutral mononuclear model molecule: (**a**) **1**; (**b**) **2** (right). The yellow transparent surface shows calculated directional dependence of molecular magnetization.

Therefore, more appropriate Griffith-Figgis Hamiltonian was employed instead [19,38,66], which in atomic units adopts the form of Equation (1).

$$\hat{H} = \sigma\lambda\,\vec{\hat{L}}\cdot\vec{\hat{S}} + \sigma^2\Delta_{ax}\left(\hat{L}_z^2 - \hat{L}^2/3\right) + \sigma^2\Delta_{rh}\left(\hat{L}_x^2 - \hat{L}_y^2\right) + \left(\sigma\vec{\hat{L}} + g\,\vec{\hat{S}}\right)\cdot\vec{B} \qquad (1)$$

Here $\vec{\hat{L}}$ and $\vec{\hat{S}}$ are vector operators of angular momentum and spin, respectively, and $\vec{B}$ is vector of magnetic field. Parameters of the model are the constant of spin-orbit interaction λ, combined parameter σ (accounting for covalence of chemical bonds between central ion and ligands along with configuration interaction between ground and excited terms of matching symmetry), parameter of crystal field of axial symmetry Δ_{ax}, parameter of crystal field of rhombic symmetry Δ_{rh} and gyromagnetic factor g which was fixed equal to 2.00. In this Hamiltonian the convention with σ^2 absorbed in to Δ_{ax} and Δ_{rh} can be often encountered [66]. To improve the agreement between the model and experiment the effect of molecular field was included in the fitting procedure (quantified by parameter zj). The optimum values of parameters Δ_{ax}, Δ_{rh}, σ and λ obtained from fitting of experimental curves are collected in Table 1 and the match of experimental and optimum fit curves is displayed in Figure 2. The product of error residuals $R(\chi T) \times R(M)$ gains value considerably lower than 0.05 indicating very good accordance between model and experiment. The values resulting from ab-initio calculation are collected in Table 2. Comparing the calculated and fitted values, a satisfactory agreement can be concluded for the constant of spin-orbit interaction and parameter of crystal field of axial symmetry, for the parameter of rhombic splitting; however, there is a discrepancy of one order of magnitude in the case of couple **I/1**. Since the values obtained as optimum fit of experimental data (Table 1) are model-dependent and simultaneous fit for **II** is not perfect, the values obtained by ab-initio calculation (Table 2) can be considered somewhat more reliable. Finally, the visual assessment of directional dependence of molecular magnetization derived from all SA-CAS[7,5]SCF-NEVPT2-SOI states [38,67] shows, that magnetic anisotropy is of axial-like type (which is in accordance with negative value of parameter Δ_{ax}) and that the preferred orientation of molecular magnetization is towards the connecting bridge (Figure 3).

Table 1. Magnetic parameters extracted from optimum fit for complexes **I** and **II**.

Complex	λ/cm^{-1}	σ	Δ_{ax}/cm^{-1}	Δ_{rh}/cm^{-1}	zj/cm^{-1}	$R(\chi T) \times R(M)$
I	−177.4	−1.14	−424.7	−11.6	−0.06	0.0006
II	−161.5	−1.39	−395.1	−92.1	0.007	0.0094

Table 2. Calculated magnetic parameters for model molecules **1** and **2**.

	λ/cm^{-1}	Δ_{ax}/cm^{-1}	Δ_{rh}/cm^{-1}
1	−175.3	−522.7	−151.2
2	−175.2	−425.3	−128.8

2.5. Dynamic Magnetic Properties

To examine the presence of the slow relaxation of magnetization (SRM), which is the proof of SIM behaviour, the temperature and frequency dependence of the alternating-current (AC) susceptibility was measured at low temperatures for both complexes (see Supplementary Materials, Tables S10 and S11 for a detailed experimental description of AC susceptibility measurements and data analysis). The DC field scan for a limited number of frequencies over four orders of magnitude shows that out-of-phase component of AC susceptibility is silent at $B_{DC} = 0$ T (Figure S19, see Supplementary Materials). This indicates very fast SRM, probably due to the quantum tunnelling of magnetization induced by hyperfine interactions with the nuclear spin and/or dipolar interactions between the spin centres in the lattice. In order to determine the optimal B_{DC} to suppress the quantum tunnelling effect, AC susceptibility measurements under various B_{DC} fields were applied at 2 K (Figure S19). Upon increasing DC field up to $B_{DC} = 0.8$ T, the out-of-phase component varies, but differently for individual frequencies. This confirms that compounds **I** and **II** show field-induced SRM and the subsequent temperature and frequency dependent measurements were carried out by choosing B_{DC} fields at which the out-of-phase components

χ'' reach the maximal response (B_{DC} = 0.1 T for **I** and B_{DC} = 0.2 T for **II**). Furthermore, in order to detect changes in mechanisms of the SRM upon the various static magnetic fields, the temperature variable AC susceptibility measurements have been recorded also at B_{DC} = 0.02 T for complex **I** as well as at B_{DC} = 0.05 T, B_{DC} = 0.1 T and B_{DC} = 0.15 T for complex **II** (Figures S20–S25).

At 2 K and 0.1 T, the out-of-phase component χ'' of **I** does not yet show maximum, which indicates that the SRM acquires relaxation times τ longer than 0.16 s (Figure 4a). However, the reduction of static magnetic field to 0.02 T has already caused the appearance of maxima even at the lowest temperatures of measurement (14 Hz, τ = 73 ms at 1.8 K; Figure S20, Table S12). At both fields, the increase of temperature resulted in the obvious shift of the maxima in the χ'' vs. f dependencies towards higher frequencies and proves that **I** is field-induced SIM. On the contrary, the out-of-phase component χ'' of complex **II** shows maxima around 63 Hz at 1.8 K which indicates much faster relaxation of magnetisation ($\tau \approx$ 2.54 ms) in comparison to complex **I**. Also here, the increase of temperature shifts those maxima towards higher frequencies (shorter relaxation times). All herein reported AC susceptibility measurements recorded at various static magnetic field B_{DC} were satisfactorily fitted by one-set Debye model for a single relaxation channel relaxation of magnetisation (Equations (S1) and (S2), see Supplementary Materials). This analysis resulted in the set of four parameters—adiabatic χ_S and isothermal χ_T susceptibilities, the distribution parameters α_i and relaxation times τ_i (see Supplementary Materials, Tables S12 and S13 for **I**, Tables S14–S17 for **II**).
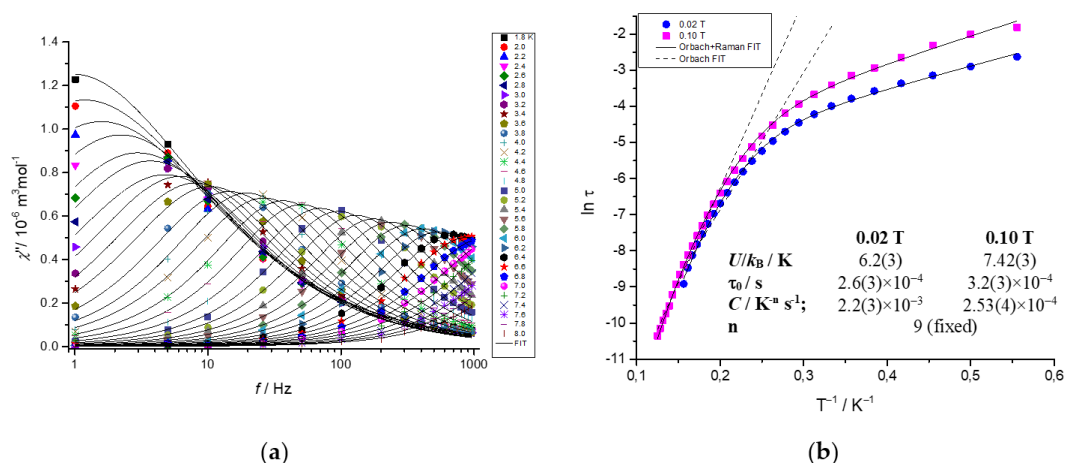

Figure 4. (**a**) Frequency dependent out-of-phase χ'' components of AC susceptibility for compound **I** recorded at the applied static magnetic field B_{DC} = 0.1 T (Solid lines present fits using the one-component Debye's model, Equations (S1) and (S2); see Supplementary Materials); (**b**) The lnτ vs. 1/T dependency obtained from AC susceptibility measurements at two static magnetic fields.

The obtained thermal dependency of relaxation time, presented in the form ln τ vs. 1/T, was analysed according to extended relaxation Equation (2) [68,69]

$$\frac{1}{\tau} = \frac{1}{\tau_0}\exp(-\frac{U}{kT}) + CT^n + AB^m T, \tag{2}$$

where the terms correspond to thermally activated Orbach, Raman and direct processes, respectively (Tables S18–S22, see Supplementary Materials). At first, the high temperature regions of ln τ vs. 1/T dependencies were fitted to the Arrhenius-like plot, which considers the Orbach relaxation process only (Figures 4b and 5b, dashed lines). Such simple analysis resulted in the preliminary evaluation of the effective energy barrier of spin reversal U, which in the case of **I** showed a decrease upon the increase of the B_{DC} from 0.02 T (U = 52 K) to 0.1 T (U = 38 K). On the other hand, complex **II** shows field-independent

values that are twice as small (U = 26 K) in the range 0.1–0.2 T, while the linear fit of the low field measurement at 0.05 T has not yielded reliable results (Table S18).
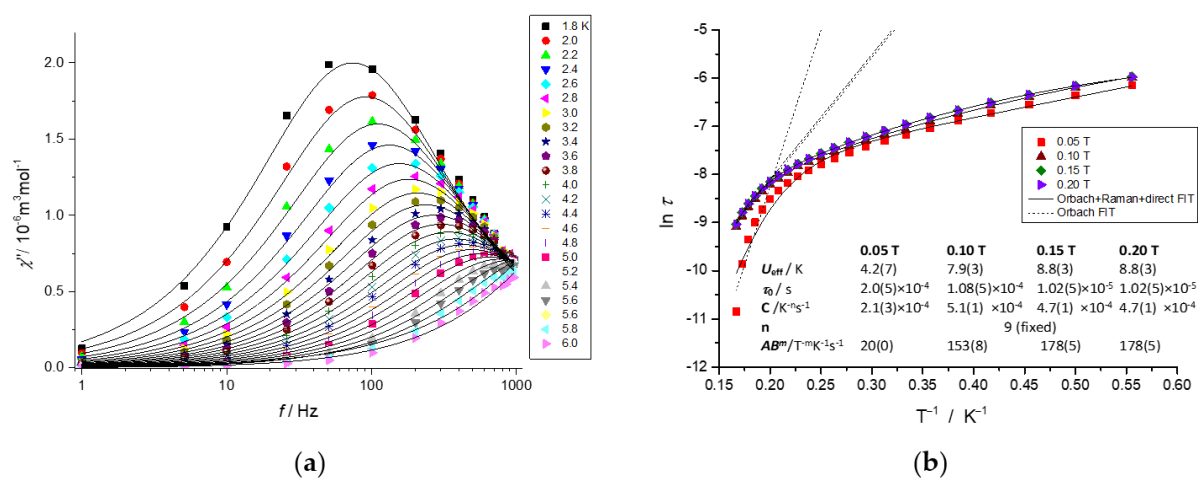

Figure 5. (**a**) Frequency dependent out-of-phase χ'' components of AC susceptibility for compound **II** recorded at the applied static magnetic field B_{DC} = 0.05 T (Solid lines present fits using the one-component Debye's model, Equations (S1) and (S2); see Supplementary Materials); (**b**) The $\ln\tau$ vs. $1/T$ dependency obtained from AC susceptibility measurements at four static magnetic fields.

In the more complex analysis of $\ln\tau$ vs. $1/T$ dependencies, combinations of two or all three relaxation processes from Equation (2) have been used for the fitting procedure (Tables S18–S22, see Supplementary Materials). The most reliable results were obtained for the combination of Orbach and Raman processes in the case of complex **I** and for the combination of all three relaxation processes in the case of complex **II** (Figures 4b and 5b) [68,69].

Although the contribution of Orbach process to the overall slow relaxation magnetisation in hexacoordinated Co(II) complexes is quite rare [70], some recent studies suggest that this two-phonon thermally activated relaxation can be operative also in this type of SIMs [70,71]. Obtained values of energy barriers U are relatively small for the class of hexacoordinated Co(II) single-ion magnets [67,71,72]. The values of Raman exponent were fixed to the recommended value n = 9 for Kramers' systems, pre-exponential constant C are rather field independent and pre-exponential factor of direct process A (if m = 4 for Kramers' system [68,69]) has an decreasing trend when the static magnetic field is increased.

To put the observed changes in magnetic relaxation in context with the change of geometry of coordination environment, the difference of symmetry measure parameter S(O_h) from 0.198 (**I**) to 0.306 (**II**) is associated with decrease of relaxation time limit τ_0 from 3.2×10^{-4} s to 1.0×10^{-5} s at the field of 0.1 T. For comparison, a recent work by Liu et al. [73] reported the effect of subtle geometry changes in isolated octahedral complexes with the same coordination environment CoN_2O_4 but an easy-plane magnetic anisotropy. In their work, the difference of symmetry measure parameter from S(O_h) = 0.025 (Co1) and S(O_h) = 0.067 (Co2) to S(O_h) = 0.117 induced a small increase of relaxation time limit τ_0 from 1.67×10^{-8} s to 1.88×10^{-8} s at the field of 0.2 T.

3. Materials and Methods

3.1. Chemical Reagents

The chemicals were of reagent grade (Sigma-Aldrich, Darmstadt, Germany) and used without further purification. The organic reagents were purchased from Sigma-Aldrich (Darmstadt, Germany) and TCI Chemicals (Tokyo, Japan); their purity was checked by IR spectra.

3.2. Syntheses of the Complexes

3.2.1. Synthesis of $\{[Co(\mu_2\text{-suc})(nia)_2(H_2O)_2]\cdot 2H_2O\}_n$ (Complex **I**)

(a)   From nicotinamide (nia)

Crystals of $\{[Co(\mu_2\text{-suc})(nia)_2(H_2O)_2]\cdot 2H_2O\}_n$ (**I**) were obtained by dissolving cobalt(II) nitrate hexahydrate (2 mmol) with equimolar quantity of sodium succinate hexahydrate in 20 cm^3 of water. Nicotinamide (4 mmol) was dissolved in 20 cm^3 of *n*-pentanol. This solution was slowly added to an aqueous solution of cobalt(II) nitrate and Na_2suc·6H_2O (Scheme 1). The resulting solution was refluxed for 1 h and during the reflux the precipitate was formed. Then the solution was slowly cooled down. The solution was filtered and two layers were created—a layer of pink water solution, which was covered by *n*-Pentanol. These two layers were left to slowly diffuse at ambient temperature. After several weeks purple crystals of complex **I** were filtered off.

Yield: 54% based on Co. Elemental analysis for $C_{16}H_{24}CoN_4O_{10}$ (M_W = 491.32) found % (expected %): C 38.7 (38.3); N 11.0 (10.8); H 4.9 (4.7); Co 12.11 (12.30). IR (ATR, cm^{-1}): 3424 sh, 3367 s, 3202 s, 3060 w, 2988 w, 2955 w, 1661 vs, 1559 vs, br, 1395 s, 1367 vs, 1151 m, 1138 m, 780 m, 652 vs, 516 vs. Electronic spectra (nujol mulls, nm): 223, 265, 330 sh, 480, 495 sh.

(b)   From *N*-(hydroxylmethyl)nicotinamide (hmnia)

Complex $\{[Co(\mu_2\text{-suc})(nia)_2(H_2O)_2]\cdot 2H_2O\}_n$, which has the same composition as complex **I**, was prepared by reaction of cobalt(II) chloride hexahydrate (2 mmol) with disodium succinate hexahydrate (2 mmol) and *N*-(hydroxymethyl)nicotinamide—hmnia (4 mmol) in 50 cm^3 of water (Scheme 2). The resulting solution was stirred under reflux. After 20 min of reflux the colour of the solution changed to purple and after another 20 min the colour changed to pink and a light precipitate was formed. After 2 h of reflux, the solution was slowly cooled down. The precipitate was filtered off and pink solution was left to evaporate at ambient temperature. After few days, purple crystals of complex $\{[Co(\mu_2\text{-suc})(nia)_2(H_2O)_2]\cdot 2H_2O\}_n$ were collected.

Yield: 48% based on Co. Elemental analysis for $C_{16}H_{24}CoN_4O_{10}$ (M_W = 491.32) found % (expected %): C 38.8 (38.3); N 11.3 (10.8); H 5.1 (4.7); Co 12.2 (12.3). IR (ATR, cm^{-1}): 3430 sh, 3360 sh, 3200 vs, 3061 w, 2989 w, 2959 w, 1656 s, 1597 s, 1546 vs, br, 1395 s, 1366 s, 1150 m, 1133 m, 779 m, 652 vs, 515 vs. Electronic spectra (nujol mull, nm): 208, 267, 325 sh, 480, 506 sh.

3.2.2. Synthesis of $[Co(\mu_2\text{-fum})(nia)_2(H_2O)_2]_n$ (Complex **II**)

Pink crystals of $[Co(\mu_2\text{-fum})(nia)_2(H_2O)_2]_n$ (**II**) were acquired by dissolving cobalt(II) nitrate hexahydrate (2 mmol), disodium fumarate (2 mmol) and nicotinamide (4 mmol) in 50 cm^3 mixture of water and methanol (1:1). Solution was refluxed for 2 h (Scheme 1). After 20 min of reflux the precipitate was formed. After 2 h, the solution was slowly cooled down and a pink precipitate was filtered off. The resulting pink solution was left to evaporate at ambient temperature. Pink crystals of complex $[Co(\mu_2\text{-fum})(nia)_2(H_2O)_2]_n$ were separated after few weeks.

Yield: 61% based on Co. Elemental analysis for $C_{16}H_{18}CoN_4O_8$ (M_W = 453.27) found % (expected %): C 41.8 (42.4); N 12.1 (12.4); H 4.2 (4.0); Co 12.2 (12.4). IR (ATR, cm^{-1}): 3500 m, 3312 s, 3193 s, br, 3060 w, 1687 s, 1622 m, 1595 sh, 1573 vs, 1557 vs, 1393 s, 1368 vs, 1153 m, 1099 m, 754 m, 653 vs, 638 vs, 504 vs. Electronic spectra (nujol mull, nm): 229, 265, 320 sh, 472, 506 sh.

3.3. Analysis and Physical Measurements

Analytical grade (Mikrochem, Pezinok, Slovakia; Acros Organics, Geel, Belgium and TCI Chemical, Tokyo, Japan) chemicals and solvents were used without further purification. Cobalt was determined by electrolysis after mineralization of the complexes; carbon, hydrogen and nitrogen were determined by microanalytical methods (Thermo Electron Flash EA 1112). Electronic spectra (9000–50,000 cm^{-1}) of the powdered samples in nujol

mull were recorded at room temperature on Specord 240 spectrophotometer (Carl Zeiss, Jena, Germany). Infrared spectra in the region of 400–4000 cm^{-1} were recorded on a Nicolet 5700 FT-IR spectrometer (Thermo Scientific, Waltham, MA, USA). Spectra of the solid samples were obtained by ATR technique at room temperature. Magnetism of all complexes was measured using a SQUID magnetometer (MPMS-XL7, Quantum Design, San Deigo, CA, USA). The temperature dependence of magnetization was recorded at a constant magnetic field B = 0.1 (complex **I**) T or B = 0.5 T (complex **II**), corrected for diamagnetic contribution, and displayed as the product of temperature and molar susceptibility (in the cgs-emu unit system). The dependence of magnetization on the magnetic field was measured at two constant temperatures: T = 2.0 K and T = 4.6 K (complex **I**) or T = 2.0 K and T = 4.0 K (complex **II**).

3.4. Computational Details

Fitting of the DC magnetic susceptibility and magnetization of both compounds was performed with the program PHI 3.1.3 [74]. Fitting of AC magnetic susceptibility was realized with the help of a home-made program. Calculations of magnetic exchange coupling parameter was performed within ORCA 5.0.2 [75] using model molecules **11** and **22** (Figure S18, see Supplementary Materials), all other calculations were carried out within the program ORCA 4.2.0 [76] with the model molecules **1** and **2** (Figures 3 and S17, see Supplementary Materials). Magnetic coupling was assessed with exchange-correlation density functional approximations B3LYP [77–79], PBE0 [80] and TPSSh [81]. The resolution of identity and chain-of-spheres approximations for Coulomb and exchange integrals (RIJCOSX) [82] were set on. For all atoms the Ahlrichs' basis set def2-TZVP [83,84] was used with an auxiliary basis set def2/J [85]. Prior to this calculation, the positions of all hydrogen atoms were optimized on the model molecules **11** and **22** using the method PBEh-3c [86] and all other atoms were kept in their positions as obtained from the X-ray analysis. The energy levels of crystal-field terms in mononuclear model molecules **1** and **2** were obtained using the state averaged complete active space self-consistent field method (SA-CAS[7,5]SCF) [87] complemented by strongly-contracted *N*-electron valence perturbation theory of second-order (NEVPT2) [88–90] and spin-orbit interaction [91,92]. All 10 spin quartet states and 40 spin doublet reference states were taken into account. The resolution of identity approximation for Coulomb and exchange integrals (RI-JK) [82] were set on. For all atoms the basis set def2-TZVP was used, this time with an automatically generated auxiliary basis set [93]. In all calculations the increased integration grid was set (level 5 in ORCA convention). The positions of all hydrogen atoms were optimized on the model molecules **1** and **2** using the same approach as for **11** and **22**. The molecular magnetization isosurface was visualized by a home-made program using the approach described in [38]. The infrared spectra were calculated at model molecules **1** and **2** with the abovementioned basis set and hybrid exchange-correlation density functional approximation B3LYP [77–79]. No negative vibration frequencies were obtained. The electronic spectra were calculated for molecules **1** and **2** using the time-dependent DFT method with the same setting of basis and exchange-correlation functional like it was for the IR spectra, asking for 15 roots.

3.5. Crystal Structure Determination

Data collections and cell refinement were carried out using four-circle diffractometer STOE StadiVari using Pilatus3R 300K HPD detector, and microfocused X-ray source Xenocs Genix3D Cu HF (CuK_α radiation) at 100 K. The diffraction intensities were corrected for Lorentz and polarization factors. The absorption corrections were made by LANA [94]. The structures were solved with program SHELXT [95], and refined by the full-matrix least squares procedure of Independent Atom Model (IAM) [96] with SHELXL-2018/3 [97]. The Hirshfeld Atom Refinement (HAR) was carried out using IAM model as a starting point. The wave function was calculated using ORCA 4.2.0 software [76] with basis set def2-TZVPP [83,84] and hybrid exchange-correlation functional PBE0 [80]. The least-squares refinements of HAR model were then carried out with olex2.refine [98], while keeping the

same constrains and restrains as for the SHELXL refinement. The NoSpherA2 implementation [99] of HAR makes used for tailor-made aspherical atomic factors calculated on-the-fly from a Hirshfeld-partitioned electron density. For the HAR approach, all H atoms were refined isotropically and independently. All calculations and structure drawings were done in the OLEX2 package [100]. Final crystal data and HAR's refinement parameters are given in Table S1 (see Supplementary Materials).

Hirshfeld Surface Analysis

The software Crystal Explorer [101] was used to calculate Hirshfeld surface [102,103] and associated fingerprint plots [104,105]. The Hirshfeld surfaces were obtained using CIF files from HAR model.

3.6. Powder X-ray Analysis

PXRD data of **I** were collected within the 2Θ range 3°–60° on a Brag-Brentano focusing powder diffractometer PHILIPS, model 1730/10. The instrument was equipped with X-ray tube providing Co α radiation, wavelength (0.179021 nm). The experimental conditions were as follow: exciting voltage: 40 kV, anode current: 35 mA, step size: 0.02°, time on step 2.4 s.

In the case of **II**, PXRD were collected within the 2Θ range 5°–60° on a Brag-Brentano automated focusing powder diffractometer EMPYREAN. The instrument was equipped with X-ray tube providing Cu Kα radiation. wavelength (0.15405980 nm) and PIXcel3D-Medipix3 1×1 detector. The exciting voltage was 45 kV, and the anode current was 40 mA, continuous mode was used.

The simulated powder patterns of **I** and **II** were obtained from single-crystal data employing the Le Bail analysis in the computer program Jana 2006 [106].

4. Conclusions

In conclusion, we have thoroughly reinvestigated two previously described analogous cobalt (II) coordination polymers, where the isolated metal centres are bridged by succinate or fumarate anion. The molecular structures of both compounds were determined with much higher accuracy then before, showing the shortest intermetallic distances in **I** and **II** about 9.5 Å and 9.7 Å, respectively, which imply isolated magnetic environments for both systems.

Static magnetic studies and ab-initio calculations further supported that the Co(II) centres can be considered magnetically isolated and they both show easy axis magnetic anisotropy pointing towards the connecting bridge.

The AC magnetic study showed that the fumarate analogue **II** relaxes comparatively faster at the field 0.1 T than the succinate complex **I**. Although the slow relaxation of magnetization is very susceptible to even small changes in local anisotropy of coordination environment, we can suppose that the enhanced rigidity of the bridge is a non-negligible factor for conservation of molecular magnetization. Indeed, as discussed in a few recent works [107–109], magnetic relaxation is faster if the material possesses low-lying avoided-crossing points between acoustic and optical phonons, or, in simpler words, if the collective thermal vibrations spread easily to vibrations around the magnetic centre. In this sense we can state that in the studied couple of SIMs, the fumarate bridge could act as better "transmitter" of the vibrational perturbations onto the magnetic centre than the succinate bridge. We can thus conjugate that the less stiff bridges are more appropriate components for targeted design of single-molecule magnets.

Figures S20–S25: AC susceptibility data at various fields; Tables S1–S4: Crystallographic data and parameters; Tables S5–S6: Characteristic band in IR spectra; Table S7: Calculated bands in electron spectra; Table S8: Calculated magnetic coupling interaction; Table S9: Calculated energies of Kramers' doublets; Tables S10 and S11: Conditions of AC magnetic experiments; Tables S12–S17: Parameters of the extended one-set Debye model, Tables S18–S22: Relaxation parameters using various combinations of mechanisms.

Author Contributions: Conceptualization, J.P. and P.S.; syntheses, M.B.; crystallographic measurements and interpretation, J.M.; spectroscopic measurements and interpretation, M.B. and P.S.; magnetism measurements, Ľ.D. and M.K.; magnetism interpretation, J.J., I.Š. and J.P.; computational studies. J.P.; writing—original draft preparation, M.B., J.M., I.Š., J.P. and P.S.; writing—review and editing, J.P.; supervision, J.P. and P.S. All authors have read and agreed to the published version of the manuscript.

Institutional Review Board Statement: Not applicable.

Informed Consent Statement: Not applicable.

Data Availability Statement: Not applicable.

Conflicts of Interest: The authors declare no conflict of interest.

References

1. Wang, C.-C.; Li, J.-R.; Lv, X.-L.; Zhang, Y.-Q.; Guo, G. Photocatalytic organic pollutants degradation in metal-organic frameworks. *Energy Environ. Sci.* **2014**, *7*, 2831–2867. [CrossRef]
2. Lee, J.; Farha, O.K.; Roberts, J.; Scheidt, K.A.; Nguyen, S.T.; Hupp, J.T. Metal-organic framework materials as catalysts. *Chem. Soc. Rev.* **2009**, *38*, 1450–1459. [CrossRef] [PubMed]
3. Reinsch, H.; van der Veen, M.A.; Gil, B.; Marszalek, B.; Verbiest, T.; de Vos, D.; Stock, N. Sctructures, Sorption Characteristics, and Nonlinear Optical Properties of a New Series of Highly Stable Aluminum MOFs. *Chem. Mater.* **2013**, *25*, 17–26. [CrossRef]
4. Khan, S.; Masum, A.A.; Giri, P.; Islam, M.; Harms, K.; Chattopadhyay, S. Chirality-Induced Variation In Interaction of Two Similar Copper(II) Coordination Polymers with Calf Thymus DNA: Exploration of Their Antimicrobial Activity and Cytotoxicity. *Chem. Select.* **2018**, *3*, 7112–7122. [CrossRef]
5. Li, J.-R.; Kruppler, R.J.; Zhou, H.-C. Selective gas adsorption and separation in metal-organic frameworks. *Chem. Soc. Rev.* **2009**, *38*, 1477–1504. [CrossRef] [PubMed]
6. Li, L.; Wang, X.; Liang, J.; Huang, Y.; Li, H.; Lin, Z.; Cao, R. Water-Stable Anionic Metal-Organic Framework for Highly Selective Separation of Methane from Natural Gas and Pyrolysis Gas. *ACS Appl. Mater. Interfaces* **2016**, *8*, 9777–9781. [CrossRef]
7. Wilmer, C.E.; Farha, O.K.; Yildimir, T.; Eryazici, I.; Krungleviciute, V.; Sarjeant, A.A.; Snurr, R.Q.; Hupp, J.T. Gram-scale, high-yield synthesis of a robust metal-organic framework for storing methane and other gases. *Energy Environ. Sci.* **2013**, *6*, 1158–1163. [CrossRef]
8. Beauvais, L.G.; Shores, M.P.; Long, J.R. Cyano-Bridged Re_6Q_8 (Q = S, Se) Cluster-Cobalt(II) Framework Materials: Versatile Solid Chemical Sensors. *J. Am. Chem. Soc.* **2000**, *122*, 2763–2772. [CrossRef]
9. Jianghua, H.; Jihong, Y.; Yuetao, Z.; Qinhe, P.; Ruren, X. Synthesis, Structure, and Luminescent Property of a Heterometallic Metal−Organic Framework Constructed from Rod-Shaped Secondary Building Blocks. *Inorg. Chem.* **2005**, *44*, 9279–9289.
10. Kahn, O. Chemistry and Physics of Supramolecular Magnetic Materials. *Acc. Chem. Res.* **2000**, *33*, 647–657. [CrossRef]
11. Marinho, M.V.; Marques, L.F.; Diniz, R.; Stumpf, H.O.; do Canto Visentin, L.; Yoshida, M.I.; Machado, F.C.; Llorent, F.; Julve, M. Solvothermal synthesis, crystal structure and magnetic properties of homometallic Co(II) and Cu(II) chains with double di(4-pyridyl)sulfide as bridges. *Polyhedron* **2012**, *45*, 1–8. [CrossRef]

12. Zheng, Y.Z.; Evangelisti, M.; Winpenny, R.E.P. Co-Gd phosphonate complexes as magnetic refrigerants. *Chem. Sci.* **2011**, *2*, 99–102. [CrossRef]

13. James, S.L. Metal-organic frameworks. *Chem. Soc. Rev.* **2003**, *32*, 276–288.

14. Natarajan, R.; Sevitha, G.; Dominiak, P.; Wozniak, K.; Moorthy, J.N. Corundum, Diamond, and PtS Metal–Organic Frameworks with a Difference: Self-Assembly of a Unique Pair of 3-Connecting D_{2d}-Symmetric 3,3′,5,5′-Tetrakis(4-pyridyl)bimesityl. *Angew. Chem. Int. Ed.* **2005**, *44*, 2115–2119.

15. Xue, Y.-H.; Liu, Y.; Xu, D.-J. *catena*-Poly[[diaquabis(1*H*-benzimidazole-κN^3)cobalt(II)]-μ-succinato-κ*O*]. *Acta Cryst.* **2003**, *E59*, m944–m946. [CrossRef]

16. Zhang, J.; Kang, Y.; Zhang, R.-B.; Li, Z.-J.; Cheng, J.-K.; Yao, Y.-G. A twisting chiral 'dense' $7^5.9$ net, incorporating a helical sub-structure. *CrystEngComm* **2005**, *7*, 177–178.

17. Duangthonyou, T.; Jirakulpattana, S.; Phakawatchai, C.; Kurmoo, M.; Siripaisarnpipat, S. Comparison of crystal structures and magnetic properties of two Co(II) complexes containing different dicarboxylic acid ligands. *Polyhedron* **2010**, *29*, 1156. [CrossRef]

18. Bora, S.J.; Das, B.K. Synthesis and properties of a few 1-D cobaltous fumarates. *J. Solid State Chem.* **2012**, *192*, 93–101.

19. Brezovan, M.; Kuchtanin, V.; Moncoľ, J.; Pavlik, J.; Dlháň, Ľ.; Segľa, P. Four novel cobalt(II) succinate coordination polymers with *N*-heterocyclic ligands: Crystal structures, spectral properties, magnetism and computational study. *Chem. Pap.* **2020**, *74*, 3741–3753.

20. Beatty, A.M. Hydrogen bonded networks of coordination complexes. *CrystEngComm* **2001**, *3*, 243–255.

21. Beatty, A.M. Open-framework coordination complexes from hydrogen-bonded networks: Toward host/guest complexes. *Coord. Chem. Rev.* **2003**, *246*, 131–143. [CrossRef]

22. Moncoľ, J.; Kuchtanin, V.; Polakovičová, P.; Mrozinski, J.; Kalinska, B.; Koman, M.; Padělková, Z.; Segľa, P.; Melník, M. Study of copper(II) thiophenecarboxylate complexes with nicotinamide. *Polyhedron* **2012**, *45*, 94–102. [CrossRef]

23. Puchoňová, M.; Maroszová, J.; Mazúr, M.; Valigura, D.; Moncol, J. Structures with different supramolecular interactions and spectral properties of monomeric, dimeric and polymeric benzoatocopper(II) complexes. *Polyhedron* **2021**, *197*, 115050. [CrossRef]

24. Ganzhorn, M.; Wernsdorfer, W. *Molecular Magnets*; Bartolome, J., Luis, F., Fernandez, J.F., Eds.; Springer: Berlin/Heidelberg, Germany, 2014; pp. 319–364.

25. Boča, R.; Rajnák, C.; Moncol, J.; Titiš, J.; Valigura, D. Breaking the Magic Border of One Second for Slow Magnetic Relaxation of Cobalt-Based Single Ion Magnets. *Inorg. Chem.* **2018**, *57*, 14314–14321. [CrossRef] [PubMed]

26. Clérac, R.; Miyasaka, H.; Yamashita, M.; Coulon, C. Evidence for Single-Chain Magnetic Behavior in a Mn(III)-N(II) Chain Designed with High Spin Magnetic Units: A Route to High Temperature Metastable Magnets. *J. Am. Chem. Soc.* **2002**, *124*, 12837–12844. [CrossRef]

27. Frost, J.M.; Harriman, K.L.M.; Murugesu, M. The Rise of 3-d Single-Ion Magnets in Molecular Magnetism: Towards Materials from Molecules. *Chem. Sci.* **2016**, *7*, 2470–2491. [CrossRef]

28. Jiménez, J.-R.; Xy, B.; El Said, H.; Li, Y.; von Bardeleben, J.; Chamoreau, L.-M.; Lescouëzec, R.; Shova, S.; Visinescu, S.; Alexandru, M.-G.; et al. Field-induced single ion magnet behaviour of discrete and one-dimensional complexes containing [bis(1-methylimidazol-2-yl)ketone]-cobalt(II) building units. *Dalton Trans.* **2021**, *50*, 16353–16363. [CrossRef]

29. Chilton, N.E. Molecular Magnetism. *Annu. Rev. Mater. Res.* **2022**, *52*, 79–101. [CrossRef]

30. Sarkar, A.; Dey, S.; Rajaraman, G. Role of Coordination Number and Geometry in Controlling the Magnetic Anisotropy in Fe^{II}, Co^{II} and Ni^{II} Single-Ion Magnets. *Chem. Eur. J.* **2020**, *26*, 14036–14058. [CrossRef]

31. Perlepe, P.S.; Maniaki, D.; Pilichos, E.; Katsoulakou, E.; Perlepes, S.P. Smart Ligands for Efficient 3d-, 4d- and 5d-Metal Single-Molecule Magnets and Single-Ion Magnets. *Inorganics* **2020**, *8*, 39. [CrossRef]

32. Váhovská, L.; Vitushkina, S.; Potočňák, I.; Trávníček, Z.; Herchel, R. Effect of linear and non-linear pseudohalides on the structural and magnetic properties of Co(II) hexacoordinate single-molecule magnets. *Dalton Trans.* **2018**, *47*, 1498–1512. [CrossRef] [PubMed]

33. Cui, H.-H.; Zhang, Y.-Q.; Chen, X.-T.; Wang, Z.; Xue, Z.-L. Magnetic anisotropy and slow magnetic relaxation processes of cobalt(II)-pseudohalide complexes. *Dalton Trans.* **2019**, *48*, 10743–10752. [CrossRef]

34. Vallejo, J.; Castro, I.; Ruiz-García, R.; Cano, J.; Julve, M.; Lloret, F.; De Munno, G.; Wernsdorfer, W.; Pardo, E. Field-Induced Slow Magnetic Relaxation in a Six-Coordinate Mononuclear Cobalt(II) Complex with a Positive Anisotropy. *J. Am. Chem. Soc.* **2012**, *134*, 15704–15707. [CrossRef]

35. Ding, Z.-Y.; Meng, Y.-S.; Xiao, Y.; Zhang, Y.-Q.; Zhu, Y.-Y.; Gao, S. Probing the influence of molecular symmetry on magnetic anisotropy of octahedral cobalt(II) complexes. *Inorg. Chem. Front.* **2017**, *4*, 1909–1916. [CrossRef]

36. Zhang, J.; Li, J.; Yang, L.; Yuan, C.; Zhang, Y.-Q.; Song, Y. Magnetic Anisotropy from Trigonal Prismatic to Trigonal Antiprismatic Co(II) Complexes: Experimental Observation and Theoretical Prediction. *Inorg. Chem.* **2018**, *57*, 3903–3912. [CrossRef] [PubMed]

37. Chen, L.; Zhou, J.; Cui, H.-H.; Yuan, A.-H.; Wang, Z.; Zhang, Y.-Q.; Ouyang, Z.-W.; Song, Y. Slow magnetic relaxation influenced by change of symmetry ideal Ci to D3d in cobalt(II)-based single-ion magnets. *Dalton Trans.* **2018**, *47*, 2506–2510. [CrossRef] [PubMed]

38. Nemec, I.; Herchel, R.; Trávníček, Z. Two polymorphic Co(II) field-induced single-ion magnets with enormous angular distortion from the ideal octahedron. *Dalton Trans.* **2018**, *47*, 1614–1623. [CrossRef]

39. Nemec, I.; Fellner, O.I.; Indruchová, B.; Herchel, R. Trigonally Distorted Hexacoordinate Co(II) Single-Ion Magnets. *Materials* **2022**, *15*, 1064. [CrossRef]

40. Landart-Gereka, A.; Quesada-Moreno, M.M.; Díaz-Ortega, I.; Nojiri, H.; Ozerov, M.; Krzystek, J.; Palacios, M.A.; Colacio, E. Large easy-axis magnetic anisotropy in a series of trigonal prismatic mononuclear cobalt(II) complexes with zero-field hidden single-molecule magnet behaviour: The important role of the distortion of the coordination sphere and intermolecular interactions in the slow relaxation. *Inorg. Chem. Front.* **2022**, *9*, 2810–2831.

41. Roy, S.; Oyarzabal, I.; Vallejo, J.; Cano, J.; Colacio, E.; Bauza, A.; Frontera, A.; Kirillov, A.M.; Drew, M.G.B.; Das, S. Two Polymorphic Forms of a Six-Coordinate Mononuclear Cobalt(II) Complex with Easy-Plane Anisotropy: Structural Features, Theoretical Calculations, and Field-Induced Slow Relaxation of the Magnetization. *Inorg. Chem.* **2016**, *55*, 8502–8513. [CrossRef]

42. Peng, G.; Qian, Y.-F.; Wang, Z.-W.; Chen, Y.; Yadav, T.; Fink, K.; Ren, X.-M. Tuning the Coordination Geometry and Magnetic Relaxation of Co(II) Single-Ion Magnets by Varying the Ligand Substitutions. *Cryst. Growth Des.* **2021**, *21*, 1035–1044. [CrossRef]

43. Rajnák, C.; Titiš, J.; Moncol, J.; Boča, R. Effect of the distant substituent on the slow magnetic relaxation of the mononuclear Co(II) complex with pincer-type ligands. *Dalton Trans.* **2020**, *49*, 4206–4210. [CrossRef] [PubMed]

44. Woods, T.J.; Ballesteros-Rivas, M.F.; Gómez-Coca, S.; Ruiz, E.; Dunbar, K.R. Relaxation Dynamics of Identical Trigonal Bipyramidal Cobalt Molecules with Different Local Symmetries and Packing Arrangements: Magnetostructural Correlations and ab inito Calculations. *J. Am. Chem. Soc.* **2016**, *138*, 16407–16416. [CrossRef] [PubMed]

45. de Campos, N.R.; Simosono, C.A.; Landre Rosa, I.M.; da Silva, R.M.R.; Doriguetto, A.C.; do Pim, W.D.; Gomes Simões, T.R.; Valdo, A.K.S.M.; Martins, F.T.; Sarmiento, C.V.; et al. Building-up host–guest helicate motifs and chains: A magneto-structural study of new field-induced cobalt-based single-ion magnets. *Dalton Trans.* **2021**, *50*, 10707–10728. [CrossRef]

46. Demir, S.; Yilmaz, V.T.; Yilmaz, F.; Buyukgungor, O. One-Dimensional Cobalt(II) and Zinc(II) Succinato Coordination Polymers with Nicotinamide: Synthesis, Structural, Spectroscopic, Fluorescent and Thermal Properties. *J. Inorg. Organomet. Polym.* **2009**, *19*, 342–347. [CrossRef]

47. Kansız, S.; Dege, N. Synthesis, crystallographic structure, DFT calculations and Hirshfeld surface analysis of a fumarate bridged Co(II) coordination polymer. *J. Mol. Struct.* **2018**, *1173*, 42–51. [CrossRef]

48. Masárová, P.; Mazúr, M.; Segľa, P.; Moncol, J. Supramolecular assembled networks in crystal structure built up of copper(II) dipicolinates with pyrazine- and pyridinecarboxamides connected through hydrogen bonds. *Polyhedron* **2018**, *149*, 25–33. [CrossRef]

49. Shamuratov, E.B.; Batsanov, A.S.; Struchkov, Y.T.; Yunuskhodzhaev, A.N.; Dusmatov, A.F.; Sabirov, V.K. Structure of Co(II) and Cu(II) complexes with *N*-(hydroxymethyl)nicotinamide. *Russ. J. Coord. Chem.* **1990**, *16*, 1526–1528.

50. Shamuratov, E.B.; Batsanov, A.S.; Struchkov, Y.T.; Yunuskhodzhaev, A.N. Crystal structures of Ni(II) and Co(II) chloride and nitrate complexes with *N*-(hydroxymethyl)nicotinamide. *Russ. J. Coord. Chem.* **1991**, *17*, 1668–1675.

51. Chłopicki, S.; Ku, K.; Kalvins, I.; Adrianov, V.; Loza, E. Quaternary Nicotinamide Derivatives as Precursors for Release of MNA. European Patent Organization. Patent EP3505512 A1, 3 July 2019.

52. Alvarez, S.; Avnir, D.; Llunell, M.; Pinsky, M. Continuous symmetry maps and shape classification. The case of six-coordinated metal compounds. *New J. Chem.* **2002**, *26*, 996–1009. [CrossRef]

53. Alvarez, S. Relationships between Temperature, Magnetic Moment, and Continuous Symmetry Measures in Spin Crossover Complexes. *J. Am. Chem. Soc.* **2003**, *125*, 6795–6802. [CrossRef] [PubMed]

54. Alvarez, S. Distortion Pathways of Transition Metal Coordination Polyhedra Induced by Chelating Topology. *Chem. Rev.* **2015**, *115*, 13447–13483. [CrossRef]

55. Kershaw Cook, L.J.; Mohammed, R.; Sherborne, G.; Roberts, T.D.; Alvarez, S.; Halcrow, M.A. Spin state behavior of iron(II)/dipyrazolylpyridine complexes. New insights from crystallographic and solution measurements. *Coord. Chem. Rev.* **2015**, *289–290*, 2–12. [CrossRef]

56. Guionneau, P.; Marchivie, M.; Bravic, G.; Létard, J.-F.; Chasseau, D. Structural Aspects of Spin Crossover. Example of the [Fe^{II}L$_n$(NCS)$_2$] Complexes. *Top. Curr. Chem.* **2004**, *234*, 97–128.

57. Halcrow, M.A. Structure:function relationships in molecular spin-crossover complexes. *Chem. Soc. Rev.* **2011**, *40*, 4119–4142. [CrossRef]

58. Bernstein, J.; Davis, R.E.; Shimoni, L.; Chang, N.-L. Patterns in Hydrogen Bonding: Functionality and Graph Set Analysis in Crystals. *Angew. Chem. Int. Ed.* **1995**, *34*, 1555–1573. [CrossRef]

59. Janiak, C. A critical account on π–π stacking in metal complexes with aromatic nitrogen-containing ligands. *J. Chem. Soc. Dalton Trans.* **2000**, *21*, 3885–3896. [CrossRef]

60. Dziewulska-Kułaczkowska, A.; Mazur, L.; Ferenc, W. Thermal, spectroscopic and structural studies of zinc(II) complex with nicotinamide. *J. Therm. Anal. Calorim.* **2009**, *96*, 255–260. [CrossRef]

61. Nakamoto, K. *Infrared and Raman Spectra of Inorganic and Coordination Compounds, Part B*; Wiley-VCH: Weinheim, Germany, 1997; pp. 384–387; ISBN 9780471743392.

62. Bando, Y.; Nagakura, S. The electronic structure and electronic spectrum of dichlorodipyridinecobalt(II). Charge-transfer band due to interaction between halide ion and cobalt(II) cation. *Inorg. Chem.* **1968**, *7*, 893–897. [CrossRef]

63. Lever, A.B.P. *Inorganic Electronic Spectroscopy*; Elsevier: Amsterdam, The Netherlands, 1984; ISBN 0-444-42389-3.

64. Martin, R.L. Natural Transition Orbitals. *J. Chem. Phys.* **2003**, *118*, 4775. [CrossRef]

65. Palii, A.; Tsukerblatt, B.; Klokishner, S.; Dunbar, K.R.; Clemente-Juan, J.M.; Coronado, E. Beyond the Spin Model: Exchange Coupling in Molecular Magnets with Unquenched Orbital Angular Momenta. *Chem. Soc. Rev.* **2011**, *40*, 3130–3156. [CrossRef] [PubMed]

66. Boča, R. Magnetic Parameters and Magnetic Functions in Mononuclear Complexes Beyond the Spin-Hamiltonian Formalism. In *Magnetic Functions Beyond the Spin-Hamiltonian. Structure and Bonding*; Springer: Berlin/Heidelberg, Germany, 2006; Volume 117. [CrossRef]

67. Juráková, J.; Dubnická Midlíková, J.; Hrubý, J.; Kliuikov, A.; Santana, V.T.; Pavlik, J.; Moncoľ, J.; Čižmár, E.; Orlita, M.; Mohelský, I.; et al. Pentacoordinate cobalt(II) single ion magnets with pendant alkyl chains: Shall we go for chloride or bromide? *Inorg. Chem. Front.* **2022**, *9*, 1179–1194. [CrossRef]

68. Singh, A.; Shrivastava, K. Optical-acoustic two-phonon relaxation in spin systems. *Phys. Status Solidi B* **1979**, *95*, 273–277. [CrossRef]

69. Shrivastava, K.N. Theory of Spin–Lattice Relaxation. *Phys. Status Solidi B* **1983**, *117*, 437–458. [CrossRef]

70. Juráková, J.; Šalitroš, I. Co(II) single-ion magnets: Synthesis, structure and magnetic properties. *Monatsh. Chem.* 2022; *in press*. [CrossRef] [PubMed]

71. Zahradníková, E.; Herchel, R.; Šalitroš, I.; Císařová, I.; Drahoš, B. Late first-row transition metal complexes of a 17-membered piperazine-based macrocyclic ligand: Structures and magnetism. *Dalton Trans.* **2020**, *4I9*, 9057–9069. [CrossRef] [PubMed]

72. Brachňaková, B.; Matejová, S.; Moncoľ, J.; Herchel, R.; Pavlik, J.; Moreno-Pineda, E.; Ruben, M.; Šalitroš, I. Stereochemistry of coordination polyhedral vs. single ion magnetism in penta- and hexacoordinated Co(II) complexes with tridentate rigid ligands. *Dalton Trans.* **2020**, *49*, 1249–1264. [CrossRef] [PubMed]

73. Wu, Y.; Tian, D.; Ferrando-Soria, J.; Cano, J.; Yin, L.; Ouyang, Z.; Wang, Z.; Luo, S.; Liu, X.; Pardo, E. Modulation of the magnetic anisotropy of octahedral cobalt(II) single-ion magnets by a fine-tuning of axial coordination microenvironment. *Inorg. Chem. Front.* **2019**, *6*, 848–856. [CrossRef]

74. Chilton, N.F.; Anderson, R.P.; Turner, L.D.; Soncini, A.; Murray, K.S. PHI: A powerful new program for the analysis of anisotropic monomeric and exchange-coupled polynuclear *d*- and *f*-block complexes. *J. Comput. Chem.* **2013**, *34*, 1164–1175. [CrossRef]

75. Neese, F. Software update: The ORCA program system, version 5.0. *WIREs Comput Mol Sci.* **2022**, *12*, e1606. [CrossRef]

76. Neese, F. Software update: The ORCA program system, version 4.0. *WIREs Comput. Mol. Sci.* **2018**, *8*, e1327. [CrossRef]

77. Vosko, S.H.; Wilk, L.; Nusair, M. Accurate spin-dependent electron liquid correlation energies for local spin density calculations: A critical analysis. *Can. J. Phys.* **1980**, *58*, 1200–1211. [CrossRef]

78. Lee, C.; Yang, W.; Parr, R.G. Development of the Cole-Salvetti correlation-energy formula into a functional of the electron density. *Phys. Rev. B.* **1988**, *37*, 785–789. [CrossRef]

79. Becke, A.D. Density-functional thermochemistry. III. The role of exact exchange. *J. Chem. Phys.* **1993**, *98*, 5648–5651. [CrossRef]

80. Adamo, C.; Barone, V. Toward reliable density functional methods without adjustable parameters: The PBE0 model. *J. Chem. Phys.* **1999**, *110*, 6158–6169. [CrossRef]

81. Tao, J.M.; Perdew, J.P.; Staroverov, V.N.; Scuseria, G.E. Climbing the density functional ladder: Nonempirical meta-generalized gradient approximation designed for molecules and solids. *Phys. Rev. Lett.* **2003**, *91*, 146401. [CrossRef]

82. Izsák, R.; Neese, F. An overlap fitted chain of spheres exchange method. *J. Chem. Phys.* **2011**, *135*, 144105. [CrossRef]

83. Weigend, F.; Ahlrichs, R. Balanced basis sets of split valence, triple zeta valence and quadruple zeta valence quality for H to Rn: Design and assessment of accuracy. *Phys. Chem. Chem. Phys.* **2005**, *7*, 3297–3305. [CrossRef]

84. Weigend, F.; Kattanneck, M.; Ahlrichs, R. Approximated electron repulsion integrals: Cholesky decomposition versus resolution of the identity methods. *J. Chem. Phys.* **2009**, *130*, 164106. [CrossRef]

85. Weigend, F. Accurate Coulomb-fitting basis sets for H-Rn. *Phys. Chem. Chem. Phys.* **2006**, *8*, 1057–1065. [CrossRef]

86. Grimme, S.; Brandenburg, J.G.; Bannwarth, C.; Hanse, A. Consistent structures and interactions by density functional theory with small atomic orbital basis sets. *J. Chem. Phys.* **2015**, *143*, 054107. [CrossRef] [PubMed]

87. Malmqvist, P.A.; Roos, B.O. The CASSCF state interaction method. *Chem. Phys. Lett.* **1989**, *155*, 189–194. [CrossRef]

88. Angeli, C.; Cimiraglia, R.; Malrieu, J.-P. *N*-electron valence state perturbation theory: A fast implementation of the strongly contracted variant. *Chem. Phys. Lett.* **2001**, *350*, 297–305. [CrossRef]

89. Angeli, C.; Cimiraglia, R.; Evangelisti, S.; Leininger, T.; Malrieu, J.-P. Introduction of *n*-electron valence states for multireference perturbation theory. *J. Chem. Phys.* **2001**, *114*, 10252–10264. [CrossRef]

90. Angeli, C.; Cimiraglia, R.; Malrieu, J.-P. *n*-electron valence state perturbation theory: A spinless formulation and an efficient implementation of the strongly contracted and of the partially contracted variants. *J. Chem. Phys.* **2002**, *117*, 9138–9153. [CrossRef]

91. Ganyushin, D.; Neese, F. A fully variational spin-orbit coupled complete active space self-consistent field approach: Application to electron paramagnetic resonance g-tensors. *J. Chem. Phys.* **2013**, *138*, 104113. [CrossRef]

92. Neese, F. Efficient and accurate approximations to the molecular spin-orbit coupling operator and their use in molecular g-tensor calculations. *J. Chem. Phys.* **2005**, *122*, 034107. [CrossRef] [PubMed]

93. Stoychev, G.L.; Auer, A.A.; Neese, F. Automatic Generation of Auxiliary Basis Sets. *J. Chem. Theory Comput.* **2017**, *13*, 554–562. [CrossRef] [PubMed]

94. Kožíšková, J.; Hahn, F.; Richter, J.; Kožíšek, J. Comparison of different absorption corrections on the model structure of tetrakis(μ_2-acetato)-diaqua-di-copper(II). *Acta Chim. Slovaca* **2016**, *9*, 136–140. [CrossRef]

95. Sheldrick, G.M. *SHELXT*—Integrated space-group and crystal-structure determination. *Acta Cryst.* **2015**, *A71*, 3–8. [CrossRef]

96. Coppens, P.; Hansen, N.K. Testing aspherical atom refinements on small-molecule data sets. *Acta Crystallogr.* **1978**, *A34*, 909–921.

97. Sheldrick, G.M. Crystal structure refinement with *SHELXL. Acta Cryst.* **2015**, *C71*, 3–8.

98. Bourhis, L.J.; Dolomanov, O.V.; Gildea, R.J.; Howard, J.A.K.; Puschmann, H. The anatomy of a comprehensive constrained, restrained refinement program for the modern computing environment—*Olex2* dissected. *Acta Cryst. A* **2015**, *A71*, 59–75. [CrossRef] [PubMed]

99. Kleemiss, F.; Dolomanov, O.V.; Bodensteiner, M.; Peyerimhoff, N.; Midgley, L.; Bourhis, L.J.; Genoni, A.; Malaspina, L.A.; Jayatilaka, D.; Spencer, J.L.; et al. Accurate crystal structures and chemical properties from NoSpherA2. *Chem. Sci.* **2021**, *12*, 1675–1692. [CrossRef] [PubMed]

100. Dolomanov, O.V.; Bourhis, L.J.; Gildea, R.J.; Howard, J.A.K.; Puschmann, H. *OLEX2*: A complete structure solution, refinement and analysis program. *J. Appl. Cryst.* **2009**, *42*, 339–341. [CrossRef]

101. Spackman, P.R.; Turner, M.J.; McKinnon, J.J.; Wolff, S.K.; Grimwood, D.J.; Jayalitaka, D.; Spackman, M.A. *CrystalExplorer*: A program for Hirshfeld surface analysis, visualization and quantitative analysis of molecular crystals. *J. Appl. Cryst.* **2021**, *54*, 1006–1011. [CrossRef]

102. Hirshfeld, F.L. Bonded-atom fragments for describing molecular charge densities. *Theor. Chim. Acta* **1977**, *44*, 129–138. [CrossRef]

103. Spackman, M.A.; Jayalitaka, D. Hirshfeld surface analysis. *CrystEngComm* **2009**, *11*, 19–32. [CrossRef]

104. Spackman, M.A.; McKinnon, J.J. Fingerprinting intermolecular interactions in molecular crystals. *CrystEngComm* **2002**, *4*, 378–392. [CrossRef]

105. Parkin, A.; Barr, G.; Dong, W.; Gilmore, C.J.; Jayalitaka, D.; McKinnon, J.J.; Spackman, M.A.; Wilson, C.C. Comparing entire crystal structures: Structural genetic fingerprinting. *CrystEngComm* **2007**, *9*, 648–652. [CrossRef]

106. Petříček, V.; Dušek, M.; Palatinus, L.J. *The Crystallographic Computing System*; Institute of Physics: Praha, Czech Republic, 2006.

107. Lunghi, A.; Totti, F.; Sanvito, S.; Sessoli, R. Intra-molecular origin of the spin-phonon coupling in slow-relaxing molecular magnets. *Chem. Sci.* **2017**, *8*, 6051–6059. [CrossRef] [PubMed]

108. Lunghi, A.; Sanvito, S. How do phonons relax molecular spins? *Sci. Adv.* **2019**, *5*, eaax7163. [CrossRef] [PubMed]

109. Garlatti, E.; Tesi, L.; Lunghi, A.; Atzori, M.; Voneshen, D.J.; Santini, P.; Sanvito, S.; Guidi, T.; Sessoli, R.; Carretta, S. Unveiling phonons in a molecular qubit with four-dimensional inelastic neutron scattering and density functional theory. *Nat. Commun.* **2020**, *11*, 1751. [CrossRef] [PubMed]